

# NWP Model Error Structure Functions Obtained From Scatterometer Winds

Jur Vogelzang and Ad Stoffelen

**Abstract**—Wind vectors derived from scatterometer measurements are spatially detailed as compared to global numerical weather prediction (NWP) model fields. Since the Advanced Scatterometer (ASCAT)’s wind vector ambiguities are, in general, well defined, ambiguity removal results in accurate wind fields. The dense and regular spatial sampling of ASCAT winds represents a unique resource to study the NWP model field spatial error structure. The current level 2 ASCAT data processor employs 2-D variational ambiguity removal (2DVAR), in which an analysis is made from the ambiguous wind solutions and a prior NWP wind field using a variational technique, and, subsequently, the ambiguity closest to the analysis is selected as best wind. 2DVAR will yield an optimal analysis when the structure functions (background error correlations in the potential domain) are well specified. In this paper, a new method is presented to calculate structure functions from autocorrelations of observed scatterometer wind components minus NWP model predictions (O–B). It is based on direct integration of the differential equations relating structure functions and observed autocorrelations. Reprocessing ASCAT data at 12.5-km grid size with structure functions obtained this way shows a considerable increase in the spectral density of the analysis for scales from about 800 to about 100 km, with the largest effect at scales of around 250 km. In line with this finding, it is shown in a case study that a more detailed analysis leads to fewer ambiguity removal errors for ASCAT data recorded over a frontal zone with rapidly varying wind direction.

**Index Terms**—Advanced Scatterometer (ASCAT), ocean vector winds, radar remote sensing, scatterometry.

## I. INTRODUCTION

SCATTEROMETER measurements give valuable information on the ocean surface vector wind. Scatterometer backscatter measurements are accumulated over a wind vector cell (WVC), and different antennas provide generally three or four different geometrical views and/or microwave polarizations over a given WVC. WVCs are organized in a swath and, depending on the accumulation process, are typically independent over distances of more than two WVCs. Therefore, scatterometers are known to provide useful mesoscale information on the atmospheric flow. In this paper, we

characterize and analyze the spatial structures as observed by scatterometers in order to represent these in numerical analysis fields.

Inversion of the observed radar cross section multiplets using an appropriate geophysical model function yields more than one solution for the wind vector in the majority of cases. These solutions are commonly referred to as ambiguous winds or ambiguities. If scatterometer winds are to be assimilated into numerical weather prediction (NWP) models, all ambiguities, together with their *a priori* probabilities, may be fed into the data assimilation system which will choose the ambiguity that gives the best match to the model state [1]. Similarly, when the scatterometer wind field is to be used as a stand-alone product for nowcasting applications, for instance to issue high-wind warnings [2], the “best” ambiguity must be selected. This procedure is known as ambiguity removal.

Various schemes for ambiguity removal have been proposed, and the reader is referred to [3] for an overview of them. One of the more sophisticated schemes is 2-D variational ambiguity removal (2DVAR), following procedures common in meteorological analysis, such as that used in 3D-Var and 4D-Var data assimilation. 2DVAR has been implemented within the Satellite Application Facility for Numerical Weather Prediction for use in processing data from the European Remote Sensing satellite (ERS), the Advanced Scatterometer (ASCAT) on board MetOp-A, and the American SeaWinds scatterometer carried by QuikSCAT. It is also experimentally used at the Royal Netherlands Meteorological Institute (KNMI) in processing data from the Indian OSCAT scatterometer on board OceanSat-2.

2DVAR consists of two steps [3]. In the first step, an analysis of the ocean surface vector wind is made from a prior background field [usually a prediction by the European Centre for Medium-Range Weather Forecasting (ECMWF)] and the ambiguous winds, taking their *a priori* probabilities into account. In the second step, the ambiguity closest to the analysis is selected as best solution. 2DVAR can therefore also be referred to as “closest-to-analysis.” The analysis is made using the method of variational data assimilation, which evolved from statistical interpolation as described by Daley [4]. Since 2DVAR is similar to the 3DVAR and 4DVAR schemes commonly used in data assimilation, it can be seen as a simplified, though nontrivial, data assimilation system.

A variational data assimilation scheme based on statistical interpolation acts as a low-pass filter (e.g., [4] and [5]). Optimal performance of such a system is obtained when the error correlations of background and observations are well described. Fig. 1 shows wind spectra for the scatterometer winds (blue

Manuscript received May 24, 2011; revised July 15, 2011; accepted September 3, 2011. This work was supported by the European Organisation for the Exploitation of Meteorological Satellites (EUMETSAT) in the context of the Satellite Application Facility for Numerical Weather Prediction (NWP SAF).

The authors are with the Royal Netherlands Meteorological Institute (KNMI), 3732 GK De Bilt, The Netherlands (e-mail: Jur.Vogelzang@knmi.nl).

Color versions of one or more of the figures in this paper are available online at <http://ieeexplore.ieee.org>.

Digital Object Identifier 10.1109/TGRS.2011.2168407

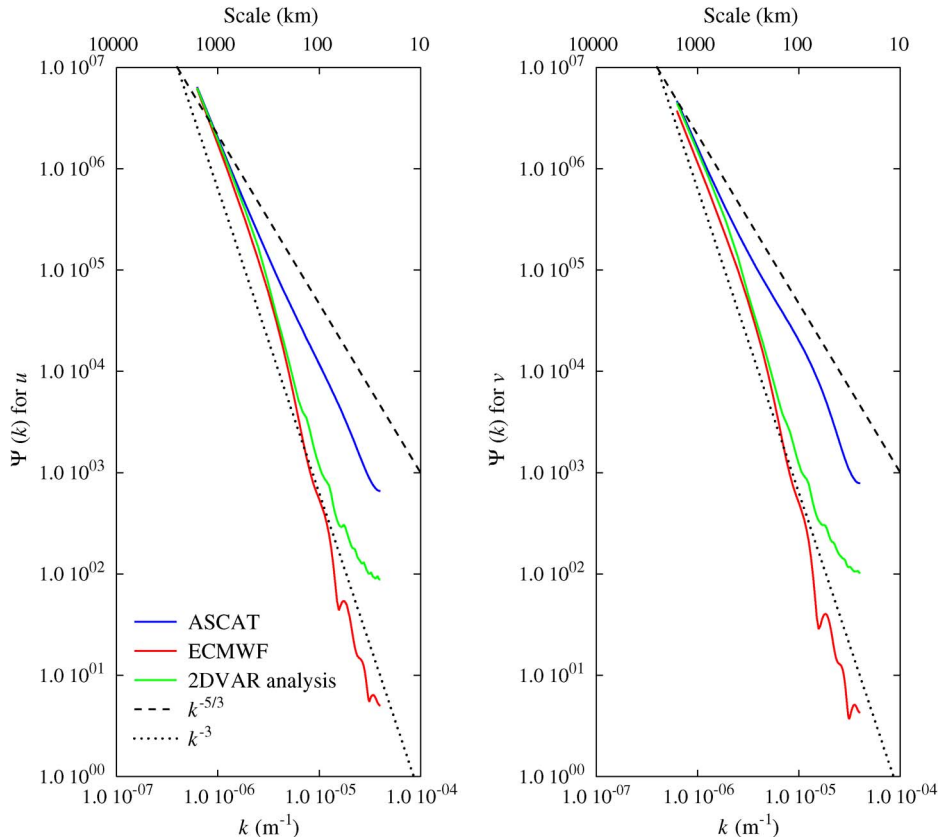


Fig. 1. Wind component spectra obtained from all ASCAT-12.5 data of January 2009.

curves), for the ECMWF background winds (red curves), and for the 2DVAR analyses (green curves). The spectra are shown as functions of wavenumber  $k$  (lower axes) and wavelength  $k^{-1}$  (upper axes). They were calculated using the methods described in [6] and [7]. The left-hand panel shows spectra for the zonal wind component  $u$ , while the right-hand panel displays that for the meridional wind component  $v$ . The black lines show theoretical spectra at arbitrary scale as predicted by Kolmogorov's turbulence theory: a  $k^{-5/3}$  spectrum for the 3-D case (dashed lines) and a  $k^{-3}$  spectrum for the 2-D case (dotted lines). The spectra in Fig. 1 were obtained using all ASCAT data on 12.5-km swath grid size and collocated ECMWF predictions from January 2009. The figure shows indeed that the 2DVAR analysis contains much less wind information on scales below about 800 km than that measured by the scatterometer, for which the spectrum is not as steep. The ECMWF background contains even less small-scale information than the 2DVAR analysis. This is presumably because of the numerical cutoff within the weather model, preventing small (unknown) disturbances to grow and degrade the model prediction skill at medium forecast range. This cutoff starts already at scales of about 800 km.

In this paper, we analyze the spatial coherence in the structures measured by scatterometers and absent in the ECMWF background. In 2DVAR, this coherence may be exploited to produce analyses that more closely follow the scatterometer observations. Moreover, since 2DVAR, 3DVAR, and 4DVAR are very similar, this paper is of relevance for mesoscale data assimilation.

Despite the spectral limitation in the 2DVAR analyses, the ASCAT spectra appear very reasonable, and ASCAT winds provide excellent buoy verification. This is because the ASCAT and ERS fan beam scatterometers basically have a dual wind direction ambiguity which is relatively easy to solve by selecting the closest to the 2DVAR analysis of two antiparallel wind vector solutions. Therefore, it is not expected that improved analyses improve the ASCAT winds a lot but rather provide a good description of the error structure in the background winds. This information is expected to be useful for the 2DVAR processing of more ambiguous scatterometer winds, such as from SeaWinds or OSCAT [1].

In this paper, the error correlations in the spatial domain are expressed in terms of the velocity potential ( $\chi$ ) and the stream function ( $\psi$ ) and are further referenced to as structure functions. The current version of 2DVAR assumes homogeneous and isotropic error correlations described by Gaussian structure functions with adjustable range and rotation/divergence ratio (see Section II).

The observation error correlations are easily and reasonably described by assuming no correlation at all. This leaves the error variances as the only unknowns. These can be obtained from statistical methods like triple collocation [6], [8]. The assumption of uncorrelated observation errors is justified in most cases, but for scatterometer measurements, some caution must be exercised (see Section II-D).

For obtaining the background error correlations, two methods exist at the moment. The first one is synthetic and employs model predictions at different prediction times to estimate the

background error correlations using a procedure similar to Kalman filtering. This method is implemented in a number of NWP models, including that of ECMWF. The second method exploits the fact that the background error correlation equals the correlated differences between observations and background (O–B) when the observation errors are uncorrelated. Hollingsworth and Lönnberg [5] binned the spatial correlations of radiosonde measurements, extrapolated it to  $r = 0$  to remove the contribution of the observation error variance, and fitted a Bessel series expansion through the binned values.

In this paper, an alternative for the second method is given using the fact that scatterometer winds are available on a dense and regular grid. This allows direct solution of the differential equations that relate the autocorrelation of the background errors to the structure functions. This paper is organized as follows. In Section II, the differential equations relating autocorrelations and structure functions are solved. The numerical implementation is presented, and the need for an additional cutoff is discussed. The resulting structure functions for the ECMWF model are presented in Section III. The improved spectral characteristics of the 2DVAR analysis and subsequent ambiguity removal are discussed. It is shown for a case with rapidly varying wind direction over a front that numerical structure functions yield more detailed analyses, resulting in fewer ambiguity removal errors compared to the default Gaussian structure functions. Some limitations of the method as well as possible solutions are discussed in Section IV. Here, it is also argued that larger effects on ambiguity removal skill may be expected for pencil beam scatterometers like SeaWinds on QuikSCAT and OSCAT on Oceansat-2. This paper ends with the conclusions in Section V.

## II. STRUCTURE FUNCTIONS

### A. Derivation

The current version of 2DVAR uses Gaussian structure functions defined in the spatial domain as

$$\rho_{\alpha\alpha}(r) = \exp\left(-\frac{r^2}{R_\alpha^2}\right) \quad (1)$$

with  $\alpha = \chi, \psi$ . The autocorrelations of the longitudinal and transversal wind components ( $\rho_{ll}$  and  $\rho_{tt}$ ) are related to the structure functions as given by Daley [5, eqs. (5.2.28) and (5.2.29)] as

$$\rho_{ll}(r) = -L_\psi^2(1-\nu^2)\frac{1}{r}\frac{d\rho_{\psi\psi}(r)}{dr} - L_\chi^2\nu^2\frac{d^2\rho_{\chi\chi}(r)}{dr^2} \quad (2a)$$

$$\rho_{tt}(r) = -L_\psi^2(1-\nu^2)\frac{d^2\rho_{\psi\psi}(r)}{dr^2} - L_\chi^2\nu^2\frac{1}{r}\frac{d\rho_{\chi\chi}(r)}{dr} \quad (2b)$$

with  $\nu^2$  being the divergence-to-rotation ratio and  $L_\psi$  and  $L_\chi$  being the length scales given by

$$L_\psi^2 = \frac{\rho_{\psi\psi}(r)}{\nabla^2\rho_{\psi\psi}(r)}\Big|_{r=0} \quad L_\chi^2 = \frac{\rho_{\chi\chi}(r)}{\nabla^2\rho_{\chi\chi}(r)}\Big|_{r=0}. \quad (3)$$

For Gaussian structure functions (1), it readily follows from (3) that  $L_\psi^2 = (1/2)R_\psi^2$  and  $L_\chi^2 = (1/2)R_\chi^2$ . This leaves  $R_\psi, R_\chi,$

TABLE I  
DEFAULT 2DVAR STRUCTURE FUNCTION PARAMETERS  
AS FUNCTION OF THE GEOGRAPHICAL LATITUDE  $\phi$

Geographical zone	$R_\psi$ (km)	$R_\chi$ (km)	$\nu^2$
NH ( $\phi > 20^\circ$ )	600	600	0.5
Tropics ( $-20^\circ < \phi < 20^\circ$ )	300	300	0.2
SH ( $\phi < -20^\circ$ )	600	600	0.5

and  $\nu^2$  as parameters determining the background error correlation. The default values in 2DVAR, originally determined for ERS, are given in Table I.

Equations (2a) and (2b) can be considered as a pair of coupled differential equations relating the observable autocorrelations  $\rho_{ll}$  and  $\rho_{tt}$  to the desired structure functions  $\rho_{\psi\psi}$  and  $\rho_{\chi\chi}$ . To solve these equations for  $\rho_{\psi\psi}$  and  $\rho_{\chi\chi}$ , they must be decoupled first. Dropping the argument  $r$  and using primes to denote the spatial derivatives, (2a) and (2b) can be rewritten as

$$\rho'_{\psi\psi} = \frac{1}{a_\psi}r\rho_{ll} - \frac{a_\chi}{a_\psi}r\rho'_{\chi\chi} \quad (4a)$$

$$\rho'_{\chi\chi} = \frac{1}{a_\chi}r\rho_{tt} - \frac{a_\psi}{a_\chi}r\rho'_{\psi\psi} \quad (4b)$$

where  $a_\psi = -L_\psi^2(1-\nu^2)$  and  $a_\chi = -L_\chi^2\nu^2$ . Substituting  $\rho_{\psi\psi}$  from (4a) into (4b) and substituting  $\rho_{\chi\chi}$  from (4b) into (4a) yields, after rearranging terms

$$\rho'''_{\psi\psi} + \frac{1}{r}\rho''_{\psi\psi} - \frac{1}{r^2}\rho'_{\psi\psi} = \frac{1}{a_\psi}\left[\frac{\rho_{tt} - \rho_{ll}}{r} + \rho'_{tt}\right] \quad (5a)$$

$$\rho'''_{\chi\chi} + \frac{1}{r}\rho''_{\chi\chi} - \frac{1}{r^2}\rho'_{\chi\chi} = \frac{1}{a_\chi}\left[\frac{\rho_{ll} - \rho_{tt}}{r} + \rho'_{ll}\right]. \quad (5b)$$

Equations (5a) and (5b) form a pair of inhomogeneous ordinary differential equations of third order. Since only derivatives in  $\rho_{\psi\psi}$  and  $\rho_{\chi\chi}$  appear, the substitutions  $X_{\psi\psi} = \rho'_{\psi\psi}$  and  $X_{\chi\chi} = \rho'_{\chi\chi}$  lead to

$$X''_{\psi\psi} + \frac{1}{r}X'_{\psi\psi} - \frac{1}{r^2}X_{\psi\psi} = g_\psi \quad (6a)$$

$$X''_{\chi\chi} + \frac{1}{r}X'_{\chi\chi} - \frac{1}{r^2}X_{\chi\chi} = g_\chi \quad (6b)$$

with  $g_\psi$  and  $g_\chi$  being given by the right-hand side of (5a) and (5b), respectively. Equations (6a) and (6b) can be solved with standard methods. The homogeneous equations are both of the Euler type, with solutions  $r$  and  $r^{-1}$ . The particular solutions are found from variation of parameters, and the integration constants are determined from the boundary conditions  $\lim_{r \rightarrow \infty} X_{\psi\psi} = 0$  and  $\lim_{r \rightarrow \infty} X_{\chi\chi} = 0$ , i.e., the derivatives of the structure functions go to zero for large distances. Straightforward integration of  $X_{\psi\psi}$  and  $X_{\chi\chi}$  with the boundary conditions  $\rho_{\psi\psi}(0) = 1$  and  $\rho_{\chi\chi}(0) = 1$  yields the final solutions

$$\rho_{\psi\psi}(r) = 1 + \frac{S(r) - R(r)}{2a_\psi} \quad (7a)$$

$$\rho_{\chi\chi}(r) = 1 + \frac{S(r) + R(r)}{2a_\chi} \quad (7b)$$

with

$$\begin{aligned}
 R(r) &= \int_0^r ds s I(s) \\
 S(r) &= \int_0^r ds \frac{J(s)}{s} \\
 I(r) &= \int_r^\infty ds \left[ \frac{\rho_{tt}(s) - \rho_{ll}(s)}{s} \right] \\
 J(r) &= \int_0^r ds s [\rho_{tt}(s) + \rho_{ll}(s)].
 \end{aligned} \tag{8}$$

$$\tag{9}$$

The parameters  $a_\psi$  and  $a_\chi$  are determined by the requirement that the structure functions approach zero as  $r$  goes to infinity as

$$a_\psi = -\frac{1}{2}(S(\infty) - R(\infty)) \quad a_\chi = -\frac{1}{2}(S(\infty) + R(\infty)). \tag{10}$$

The length scales  $L_\psi$  and  $L_\chi$  are found by substituting the solutions into (3). Since isotropy is assumed and it is also required that the autocorrelations are even functions of their argument, the Laplacian operator in (3) reduces to the second derivative, resulting in

$$L_\psi^2 = -\frac{2a_\psi}{1 - I(0)} \quad L_\chi^2 = -\frac{2a_\chi}{1 + I(0)}. \tag{11}$$

Since  $a_\psi = -L_\psi^2(1 - \nu^2)$  and  $a_\chi = -L_\chi^2\nu^2$ , it follows from (11) that

$$\nu^2 = \frac{1}{2}[1 + I(0)]. \tag{12}$$

### B. Implementation and Test

The integrals in (8) and (9) are calculated with the trapezium rule using observed autocorrelations as inputs. The structure functions and their parameters are readily calculated from (7) and (10)–(12), respectively.

For Gaussian structure functions, the corresponding autocorrelations are easily calculated analytically. These analytical autocorrelations were evaluated on a 12.5-km grid to test the algorithms. With  $R_\psi = 300$  km,  $R_\chi = 600$  km, and  $\nu^2 = 0.2$ , the resulting numerical structure functions vary between zero and one with an absolute error of 0.0024 at most. This is sufficient for our purposes.

### C. Cutoff

Numerical structure functions cannot be calculated directly from (7)–(12) when using observed autocorrelations. The reason for this is that the observed autocorrelations do not go properly to zero for large distances, as shown in Fig. 2. This is a consequence of the existence of climate zones and the finite size of the Earth. In order to let the structure functions properly go to

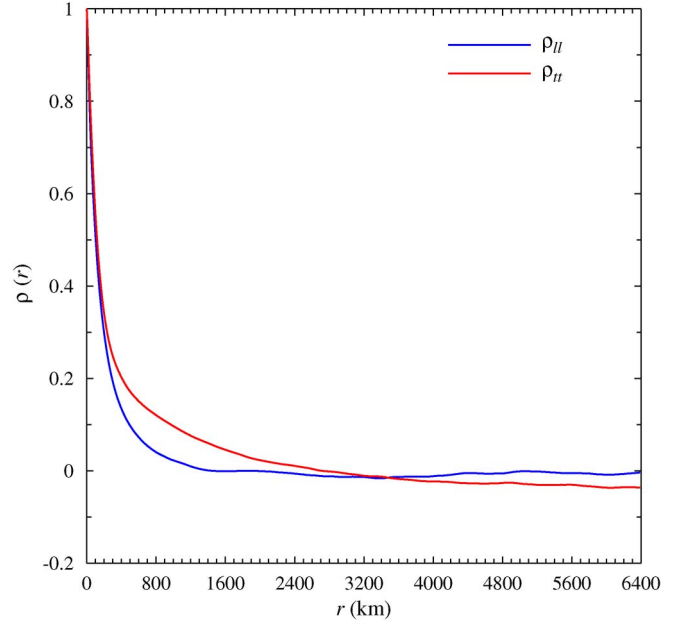


Fig. 2. Observed O–B autocorrelations for all ASCAT-12.5 data from January 2009.

TABLE II  
PARAMETERS FOR THE CUTOFF FUNCTIONS AND THE STRUCTURE FUNCTIONS RETRIEVED FROM THEM

Name	$a$ (km)	$b$ (km)	$L_\psi$ (km)	$L_\chi$ (km)	$\nu^2$
cos-3000	3000	6282	673	564	0.632
cos-4000	4000	5375	660	562	0.632
brick-wall	4700	--	658	562	0.632

zero with vanishing derivative for large distances, it is necessary to apply a cutoff function such that  $J(r) = 0$  for large  $r$ .

In this paper, the following two forms will be considered: a cosine cutoff

$$C_c(r) = \begin{cases} 1, & r < a \\ \frac{1}{2} + \frac{1}{2} \cos\left(\pi \frac{r-a}{b-a}\right), & a \leq r \leq b \\ 0, & r > b \end{cases} \tag{13}$$

and a brick-wall cutoff

$$C_b(r) = \begin{cases} 1, & r < a \\ 0, & r \geq a \end{cases} \tag{14}$$

where  $a$  and  $b$  are adjustable parameters. For the brick-wall cutoff, there is only one value for  $a$  that has the desired effect, whereas for the cosine cutoff, there is a range of  $(a, b)$  values.

Table II lists the choices made for the cutoff functions and some parameters of the resulting structure functions. Note the high values of the cutoff parameters compared to that of the range parameters for the default Gaussian structure functions in Table I. As a consequence, autocorrelations over a very long range are needed. This poses some practical problems, because the structure functions can no longer be given for the various geographical zones, as is done for the Gaussian structure functions: The tropical belt defined in Table I has a spatial extent of about 4400 km, thus limiting the maximum possible range. On the other hand, even a maximum range of 6400 km is not sufficient for successfully cutting off the autocorrelations in the extratropics. Therefore, only global results will be shown in this paper, but this point will be returned to in the discussion.

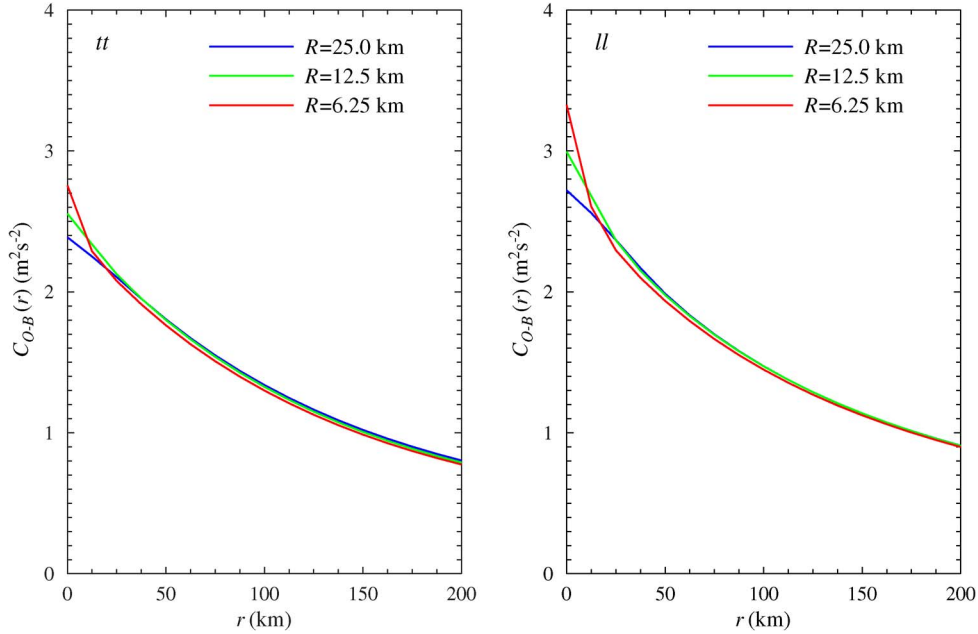


Fig. 3. O–B covariances for (left-hand panel) the transversal wind component  $t$  and (right-hand panel) the longitudinal wind component  $l$  for various choices of the averaging radius.

Application of the cutoff does not affect the autocorrelations for  $r \leq a$ .

#### D. Removal of the Observation Error Contribution

As demonstrated by Hollingsworth and Lönnberg [5], the observation error contribution to the O–B autocorrelation can be removed under the assumption that the observation errors are uncorrelated. In that case, the observation error correlation is a delta function with a contribution at  $r = 0$ . This shows up as a discontinuity at the origin in plots of autocorrelation versus distance.

The observed O–B autocorrelations in Fig. 2 show no discontinuity near the origin. This means that either the error in the ASCAT wind is negligible compared to that in the background (which contradicts the triple collocation results in [6]) or that the observation errors are correlated for ASCAT. Such a correlation originates from the fact that the radar cross section at a wind vector cell (WVC) used as input for inversion is an average over all radar measurements accumulated in an area that slightly extends beyond the WVC. For the ASCAT-12.5-km product, this area measures 50 km by 50 km and is centered with the WVC. Hamming window averaging is applied to give most weight to the central 25 km by 25 km and to minimize aliasing effects [9]. To study the effect of the size of the averaging area, the radar cross sections per WVC were recalculated from the full-resolution ASCAT level 1 product provided by the European Organisation for the Exploitation of Meteorological Satellites (EUMETSAT), averaging over a cylindrical box with adjustable size. Fig. 3 shows the O–B covariances at small distances for box radii of 6.25, 12.5, and 25 km. The autocorrelations are obtained by normalizing the covariances with their values at  $r = 0$ .

For a radius of 6.25 km, the averaging areas do not overlap, so the observation errors can be considered as weakly corre-

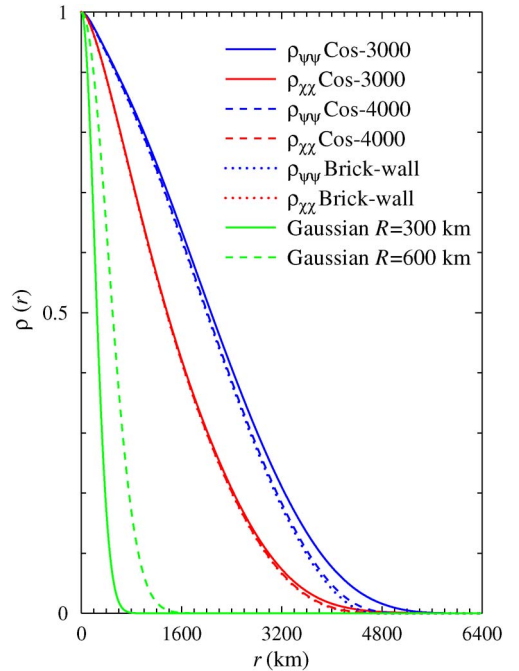


Fig. 4. Numerical structure functions calculated from autocorrelations over all Earth with (red and blue curves) various cutoff types and (green curves) analytical structure functions currently used in 2DVAR.

lated, because there may still be correlation caused by partly overlapping radar footprints that contribute to different WVCs. Since the averaging area is small, only a limited number of radar measurements contribute to the radar cross section of the corresponding WVC, resulting in considerable observation errors. As the radius increases, the observation error decreases, but the observation error correlation increases. For a radius of 25 km, the observation error seems to have vanished, but in reality, it is smeared out over a small region. Nevertheless, the difference between the various curves is small for  $r \geq 12.5$  km.

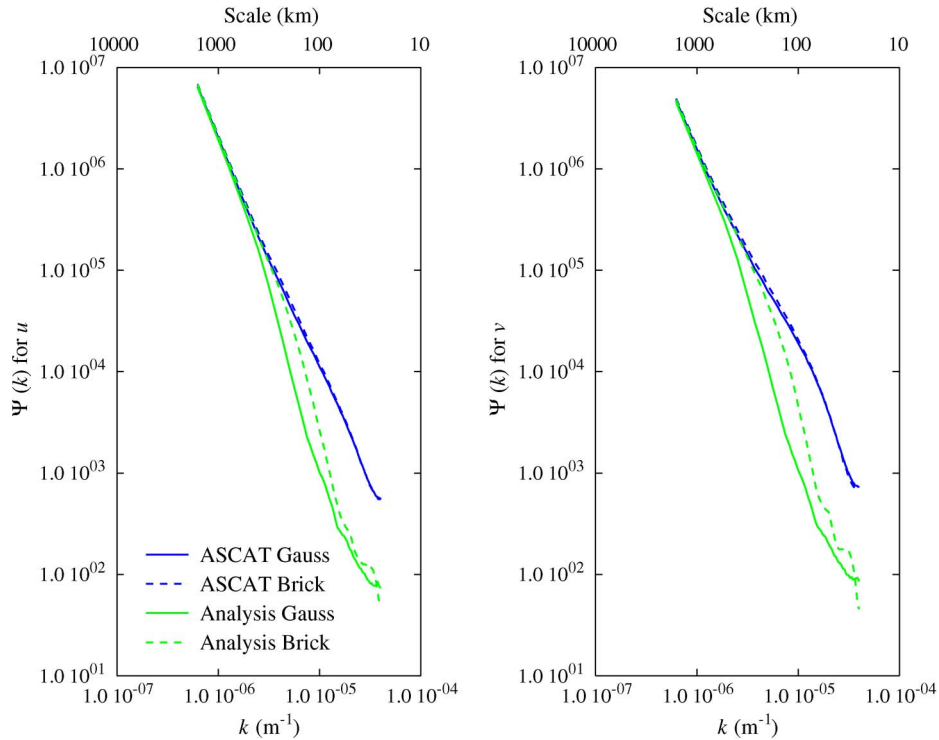


Fig. 5. Spectra of (blue curves) ASCAT-12.5 and (green curves) 2DVAR analysis for the period January 1–3, 2010, obtained with (solid curves) Gaussian structure functions and (dashed curves) numerical structure functions with brick-wall cutoff.

This suggests that the contribution of the observation error to the O–B autocorrelation is small and may be neglected.

### III. RESULTS

#### A. Shape of the Structure Functions

Fig. 4 shows the structure functions  $\rho_{\psi\psi}$  (blue curves) and  $\rho_{XX}$  (red curves) for the three cutoff functions defined in Table II. As a reference, the default Gaussian structure functions for range 300 km (solid green curve) and range 600 km (dashed green curve) are also shown. Note that the numerical structure functions are much broader than the analytical ones. In addition, the numerical  $\rho_{\psi\psi}$  is broader than the numerical  $\rho_{XX}$ , as indicated by the higher values of  $L_{\psi}$  in Table II. The choice of cutoff has little effect on  $\rho_{XX}$  and a small effect on  $\rho_{\psi\psi}$ . This is reflected in the larger spreading of  $L_{\psi}$  in Table II.

#### B. Effect on the Spectrum

Fig. 5 shows the spectra obtained for ASCAT-12.5 (blue curves) and the 2DVAR analysis (green curves) with the default Gaussian structure functions (solid curves) and the numerical structure function obtained with the brick-wall cutoff (dashed curves). The error variances of observations and background in 2DVAR were kept to their default values. Due to the long range of the numerical structure function, 2DVAR needs much more computing time, so the spectra in Fig. 5 were calculated for all ASCAT-12.5 data of January 1–3, 2009. Despite the relatively short data collection period, the spectra are an average over more than 30 000 samples. Fig. 5 shows that the numerical structure functions have a considerable impact on the analysis

TABLE III  
O–A STATISTICS OBTAINED WITH DEFAULT GAUSSIAN AND NUMERICAL STRUCTURE FUNCTIONS

Statistic	Default Gaussian		Numerical	
	$u$	$v$	$u$	$v$
Bias	-0.00110	-0.00074	-0.00080	-0.00077
Standard deviation	0.762	0.886	0.363	0.310
Minimum difference	-7.38	-7.62	-6.11	-6.23
Maximum difference	7.31	7.46	6.20	6.24

spectral density at intermediate scales. The largest effects are found for scales between 100 and 200 km. In this range, the use of numerical structure functions increases the spectral density with a factor of more than six for  $v$  and a factor of almost four for  $u$ . There is also a small impact on the ASCAT-12.5 spectrum, because a more detailed analysis may lead to better ambiguity removal. The biggest impact is a 15% increment in spectral density for spatial scales between 200 and 300 km. Note that the spectral density decreases by 10% at most for the smallest scales (40 km or less). Closer inspection of Fig. 5 reveals that both the ASCAT-12.5 spectra and the analysis spectra obtained with the default Gaussian structure functions tend to flatten at these scales, indicating the presence of noise. When using the brick-wall structure functions, 2DVAR produces an analysis with less noise at the smallest scales, causing a steeper spectral falloff. As a consequence, the ASCAT-12.5 spectra have a steeper falloff, indicating less noise at scales of 40 km and below.

A more detailed analysis of the wind fields obtained with default Gaussian structure functions and analytical ones reveals that for most WVCs, the wind vectors are the same. Therefore, the statistics of differences between ASCAT-12.5 and analysis winds are mainly due to the analysis. Table III shows the results.

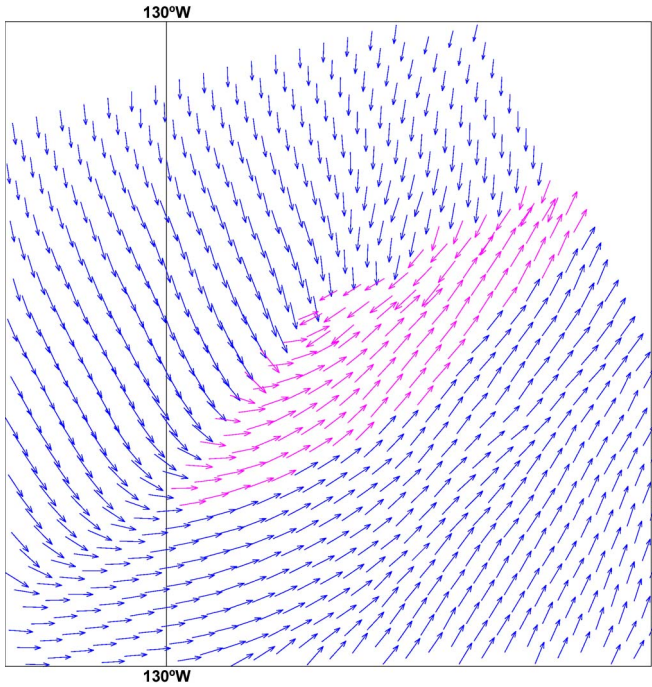


Fig. 6. ASCAT-12.5 wind field on January 2, 2009, around 5:06 UT off the west coast of Canada. Purple arrows indicate a large difference between observation and analysis. The area shown measures  $5^\circ \times 5^\circ$  centered around  $43^\circ$  N,  $129^\circ$  W.

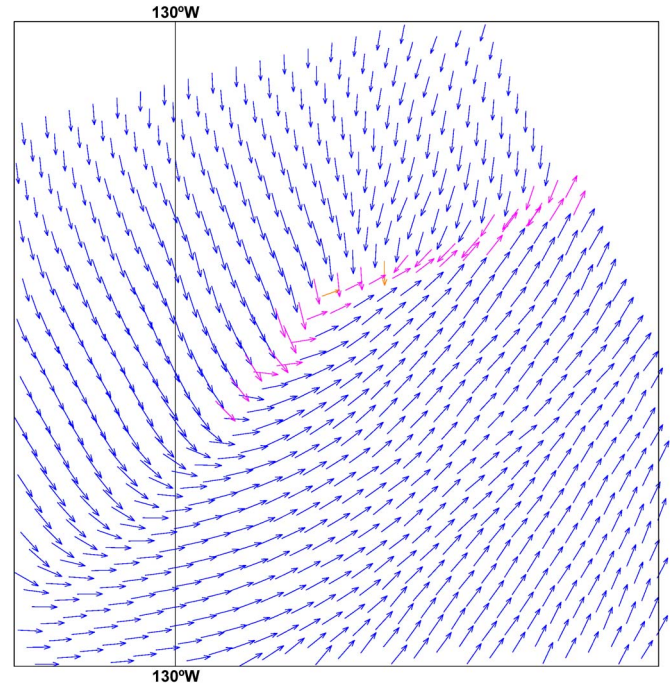


Fig. 7. Same area as Fig. 6. ASCAT-12.5 wind field obtained but obtained using numerical structure functions with brick-wall cutoff. The two orange arrows are flagged by quality control and most probably indicate rain.

The bias (average difference) remains small, while the standard deviation reduces by more than a factor of two when applying numerical structure functions instead of Gaussian ones. Moreover, the extreme differences become smaller. This shows that, indeed, the analysis improves.

### C. Effect on the Wind Field

A more detailed analysis also shows that differences in the ASCAT-12.5 wind fields occur in cases that are “difficult” for ambiguity removal: limited data close to the coast, presence of rain, large differences between observations and background, rapid changes in wind direction, or a combination of these. These findings are easy to understand, because, in most cases, the ASCAT measurements give rise to two ambiguities  $180^\circ$  apart and a more detailed analysis will have little effect on the selection. Only in cases with more than two ambiguities and particularly in the “difficult” situations mentioned before that the degree of detail in the analysis becomes critical for the selection between the ambiguities.

As an example, Fig. 6 shows the ASCAT-12.5 wind field recorded on January 2, 2009, around 5:06 UT off the west coast of Canada obtained with standard 2DVAR settings. The figure covers an area of  $4^\circ$  by  $4^\circ$  centered at  $43^\circ$  N,  $129^\circ$  W, and shows a frontal zone with a change in wind direction. The purple arrows are set by the variational quality control (VQC) and indicate a large difference between selected ambiguity and analysis. Fig. 6 shows that a large area with VQC-flagged cells is associated with the front. There are also some ambiguity removal errors, visible as  $\uparrow\downarrow$  flow patterns. Fig. 7 shows the same area as Fig. 6, but now using the numerical structure function with brick-wall cutoff. The ambiguity removal errors

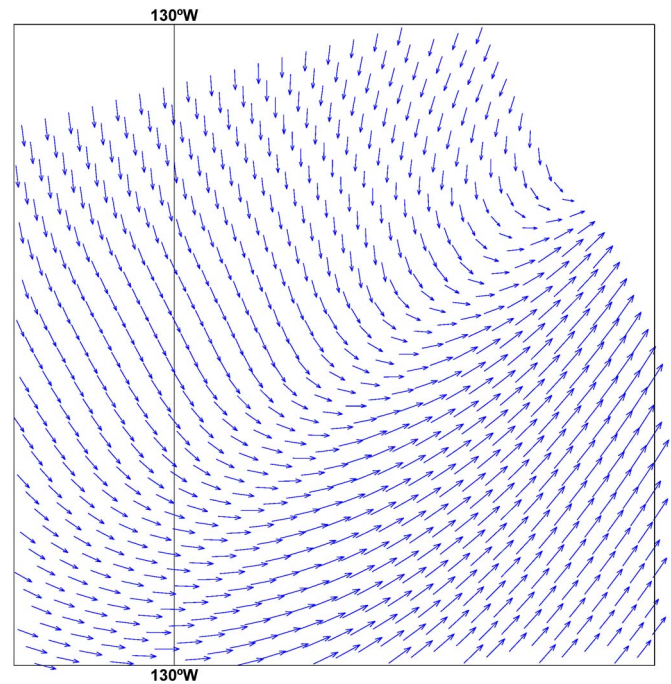


Fig. 8. ECMWF background wind on January 2, 2009, around 5:06 UT for the same area as Figs. 6 and 7.

have disappeared, and VQC flagging is restricted to a much narrower zone. Fig. 7 contains also two orange arrows. These are set by quality control and most probably indicate a confused sea state in the WVC due to the presence of variable winds. They were shown as VQC-flagged cells in Fig. 6.

The ECMWF background wind field is shown in Fig. 8. As expected, the frontal zone is represented as a wide area with gradually changing wind direction. The ECMWF background

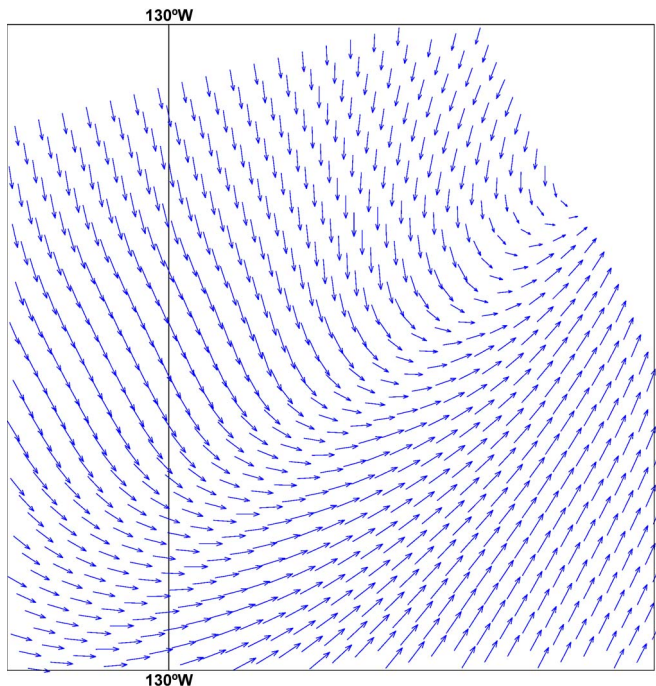


Fig. 9. Analysis obtained with default Gaussian structure functions corresponding to Fig. 6. No quality flags are shown.

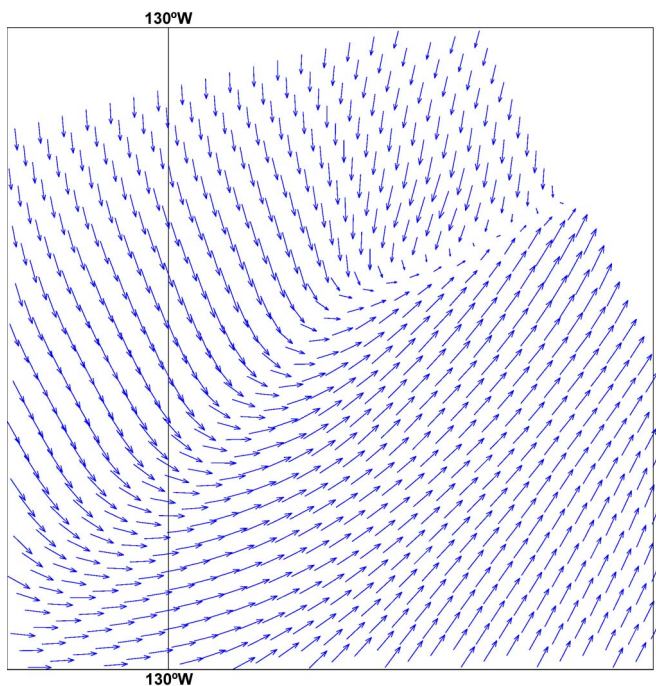


Fig. 10. Analysis obtained with numerical structure functions corresponding to Fig. 7. No quality flags are shown.

resembles the ASCAT wind field obtained with the standard Gaussian structure functions in Fig. 6. This is because the analysis, which is shown in Fig. 9, does not contain much small-scale information, while the analysis obtained with numerical structure functions, which is shown in Fig. 10, exhibits much sharper detail. Without additional wind information, it is very hard to definitely decide which wind field is correct. Nevertheless, this example demonstrates the potential of numeri-

cal structure functions for ambiguity removal in complicated situations.

#### IV. DISCUSSION

In the preceding section, it has been shown from spectral analysis and O–A statistics that numerical structure functions lead to a more detailed 2DVAR analysis from ASCAT-12.5 wind ambiguities and ECMWF predictions. This leads to modest changes in ambiguity removal, because ASCAT’s ambiguities are well defined and limited in number (usually two). However, for rotating pencil beam scatterometers like SeaWinds carried by QuikSCAT or OSCAT carried by Oceansat-2, the impact may be much larger, especially in the outer swath and the nadir swath because of the unfavorable measurement geometry there. As shown by Portabella and Stoffelen [1], this leads to broad minima in the maximum-likelihood-estimator cost function. As a consequence, the ambiguities are not well defined in wind direction. A better description is offered by retaining the full wind vector probability density function rather than a limited number of minima. This procedure is called the multisolution scheme (MSS), and it has been shown by Vogelzang *et al.* [3] that 2DVAR in combination with MSS leads to more realistic wind fields by effectively removing the measurement noise for QuikSCAT data in the nadir part of the swath.

As has been mentioned before, the results for numerical structure functions presented in this paper pertain to global structure functions. Due to the oscillatory nature of the autocorrelations, long ranges are needed to extract the structure functions from them, thus hindering inclusion of zonal effects. An alternative solution is to Fourier transform the relevant equations and to calculate the Fourier transforms of the structure functions directly from the wind spectra. Although mathematically more complicated, this seems feasible. This approach has the advantage that the wind spectrum follows a power law for large spatial frequencies that can easily be extrapolated when necessary. This will be the subject of subsequent research.

#### V. CONCLUSION

In this paper, a new method for calculating structure functions (background error correlations in terms of the wind potential and the stream function) from spatial O–B autocorrelations has been presented. The method is based on direct solution of the governing differential equations. The method is specially well suited for high-resolution satellite observations on a regular grid and is applied to ASCAT-12.5-km winds augmented with collocated ECMWF background winds. The resulting structure functions are much broader than that currently used in 2DVAR. Reprocessing ASCAT data with these structure functions leads to a considerable increase in the spectral density of the 2DVAR analysis at scales of around 100 km: by a factor of more than six for the meridional wind component  $v$  and by almost a factor of four for the zonal wind  $u$ . The analysis thus appears closer to the accurate ASCAT scatterometer observations. This is confirmed by O–A statistics: The standard deviation reduces by more than a factor of two, and the extreme differences become smaller.

As expected, the effect of the refined analysis on the 2DVAR selection is less dramatic: an increase in spectral density for scales between 200 and 300 km by 15%, indicating larger information content, and a decrease up to 10% for scales below 40 km, indicating noise reduction at the smallest scales. Changes in ambiguity removal are restricted to cases with a limited number of scatterometer data due to the coast line geometry or occasional rejection by quality control, mismatch between observations and background, or in the presence of rapid changes in wind direction. A case study over a frontal zone shows that numerical structure functions yield a much sharper frontal zone compared to the default Gaussian functions. However, more research involving additional data sources is needed to definitely verify whether numerical structure functions lead to improved ambiguity removal. Subsequent research will also address the effect on ambiguity removal performance for data from rotating pencil beam scatterometers (SeaWinds on QuikSCAT and OSCAT on Oceansat-2) and on the possibility of extracting context-dependent Fourier-transformed structure functions from wind spectra in order to examine structure functions in different meteorological conditions.

#### ACKNOWLEDGMENT

The authors would like to thank J. Patoux (Department of Atmospheric Sciences, University of Washington) for suggesting the explanation of the spectral behavior at the smallest scales in Fig. 5.

#### REFERENCES

- [1] M. Portabella and A. Stoffelen, "A probabilistic approach for SeaWinds data assimilation," *Q. J. R. Meteorol. Soc.*, vol. 130, no. 596, pp. 127–152, Jan. 2004.
- [2] J. Sienkiewicz, M. J. Brennan, R. Knabb, P. S. Chang, H. Cobb, Z. J. Jelenak, K. A. Ahmad, S. Soisuvarn, D. Kosier, and G. Bancroft, "Impact of the loss of QuikSCAT on NOAA MWS marine warning and forecast operations," in *Proc. 1st Int. Ocean Vector Winds Sci. Team Meeting*, Barcelona, Spain, May 18–20, 2010.
- [3] J. Vogelzang, A. Stoffelen, A. de Verhoef, and H. Bonekamp, "Validation of two-dimensional variational ambiguity removal on SeaWinds scatterometer data," *J. Atmos. Ocean. Technol.*, vol. 26, no. 7, pp. 1229–1245, Jul. 2010.
- [4] R. Daley, *Atmospheric Data Analysis*. Cambridge, U.K.: Cambridge Univ. Press, 1991.
- [5] A. Hollingsworth and P. Lönnberg, "The statistical structure of short-range forecast errors as determined from radiosonde data. Part I: The wind field," *Tellus*, vol. 38A, no. 2, pp. 111–136, Mar. 1986.
- [6] J. Vogelzang, A. Stoffelen, A. Verhoef, and J. Figa-Saldaña, "On the quality of high-resolution scatterometer winds," *J. Geophys. Res.*, 2011, to be published.
- [7] J. Vogelzang, How to calculate wind spectra, NWP SAF Tech. Rep. KN-TR-08, MET Office, Devon, U.K. [Online]. Available: [http://research.metoffice.gov.uk/research/interproj/nwpsaf/scatterometer/nwpsaf-tn-008\\_howtocalculatewindspectra.pdf](http://research.metoffice.gov.uk/research/interproj/nwpsaf/scatterometer/nwpsaf-tn-008_howtocalculatewindspectra.pdf).
- [8] A. Stoffelen, "Toward the true near-surface wind speed: Error modeling and calibration using triple collocation," *J. Geophys. Res.*, vol. 103, no. C4, pp. 7755–7766, 1998.
- [9] J. Figa-Saldaña, J. J. W. Wilson, E. Attema, R. Gelsthorpe, M. R. Drinkwater, and A. Stoffelen, "The Advanced Scatterometer (ASCAT) on the meteorological operational (MetOp) platform: A follow on for the European wind scatterometers," *Can. J. Remote Sens.*, vol. 28, no. 3, pp. 404–412, 2002.



**Jur Vogelzang** was born in The Netherlands on December 6, 1955. He received the M.Sc. degree in theoretical physics from the Free University, Amsterdam, The Netherlands, in 1981 and the Ph.D. degree in physics on radar remote sensing from the University of Utrecht, Utrecht, The Netherlands, in 1998.

He is currently with the Royal Netherlands Meteorological Institute (KNMI), De Bilt, The Netherlands, where he is working on scatterometer wind products.



**Ad Stoffelen** was born in The Netherlands on February 25, 1962. He received the M.Sc. degree in physics from the Technical University of Eindhoven, Eindhoven, The Netherlands, in 1987 and the Ph.D. degree in meteorology on scatterometry from the University of Utrecht, Utrecht, The Netherlands.

He is currently with the Royal Netherlands Meteorological Institute (KNMI), De Bilt, The Netherlands, where he is responsible for the Advanced Scatterometer wind products. He is also deeply involved in the European Space Agency Atmospheric Dynamics Mission-Aeolus Doppler Lidar mission.